Inorganic Chemistry

Article

pubs.acs.org/IC

# Reasons behind the Relative Abundances of Heptacoordinate Complexes along the Late First-Row Transition Metal Series

Martín Regueiro-Figueroa,[†] Luís M. P. Lima,[‡] Víctor Blanco,[§] David Esteban-Gómez,[†] Andrés de Blas,[†] Teresa Rodríguez-Blas,[†] Rita Delgado,[‡] and Carlos Platas-Iglesias*[,†]

[†]Departamento de Química Fundamental, Facultade de Ciencias, Universidade da Coruña, Campus da Zapateira-Rúa da Fraga 10, 15008 A Coruña, Spain

[‡]Instituto de Tecnologia Química e Biológica António Xavier, Universidade Nova de Lisboa, Av. da República, 2780-157 Oeiras, Portugal

[§]Departamento de Química Orgánica, Facultad de Ciencias, Universidad de Granada, Campus Fuentenueva S/N, 18071 Granada, Spain

Supporting Information

**ABSTRACT:** A series of transition metal complexes [$ML^1$] ($H_2L^1$ = 1,4,10-trioxa-7,13-diazacyclopentadecane-*N*,*N*′-diacetic acid, M = Co, Ni, Cu, or Zn) have been prepared and characterized. The X-ray structures of the [$CoL^1$] and [$CuL^1$] complexes reveal that the metal ions are seven-coordinated with a distorted pentagonal bipyramidal coordination. The five donor atoms of the macrocycle define the pentagonal plane of the bipyramid, while two oxygen atoms of the carboxylate groups coordinate apically. The [$NiL^1$] complex presents a very distorted structure with long Ni−O distances involving two oxygen atoms of the crown moiety [2.544(3) Å]. This distortion is related to the Jahn−Teller effect that is expected to operate in $d^8$ pentagonal bipyramidal complexes. The spectroscopic characterization of the [$ZnL^1$] and [$CuL^1$] complexes using NMR and EPR and the theoretical calculation of the $^{13}$C NMR shifts and *g*- and *A*-tensors using DFT confirm that these complexes retain the pentagonal bipyramidal coordination in aqueous solution. The stability trend of the [$ML^1$] complexes ($Co^{2+} > Ni^{2+} < Cu^{2+} > Zn^{2+}$), which is in contradiction with the Irving−Williams order, has been analyzed using DFT calculations (TPSSh functional). The free energy values calculated in the gas phase for [$CoL^1$](g) + [$M(H_2O)_6]^{2+}$(g) → [$ML^1$](g) + [$Co(H_2O)_6]^{2+}$(g) (M = Ni, Cu, Zn) reproduce fairly well the stability trend observed experimentally, the agreement being improved significantly upon inclusion of solvent effects. Our results indicate that the pentagonal bipyramidal coordination is particularly unfavorable for $Ni^{2+}$, and thus preorganized ligands that favor this geometry such as $L^1$ are selective for $Co^{2+}$ over $Ni^{2+}$ cations.

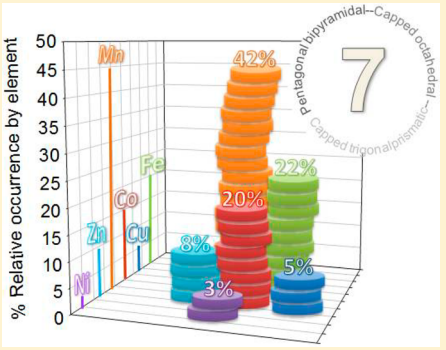


## INTRODUCTION

The most common coordination polyhedron observed for seven-coordinate first-row transition metal complexes is the pentagonal bipyramid, although capped octahedral and capped trigonal prism coordination environments have also been reported.[1] It has been shown that the distribution of seven-coordinated complexes is not uniform along the first-row transition metal series. Indeed, a search in the Cambridge Structural Database (Figure 1) shows that seven-coordination is not very common for any of the first-row transition metal series.[2−4] Seven-coordination is more abundant for Mn, Fe, and Co, for which they represent 4.5%, 1.5%, and 0.8% of the total number of structures reported. On the other hand, seven-coordinate complexes of Ni are particularly rare, and they amount only to 0.08% of the total number of hits, while for Cu and Zn heptacoordinated complexes represent 0.12% and 0.35% of the total number of structures. For instance the well-known $H_4$edta ligand ($H_4$edta = ethylenediaminetetraacetic acid) and related derivatives are known to form seven-coordinate complexes with $Mn^{2+}$, $Fe^{2+}$, and $Fe^{3+}$ having pentagonal bipyramidal or capped trigonal prismatic coordination environments, while the corresponding complexes with $Ni^{2+}$ are six-coordinated.[5] The lower presence of seven-

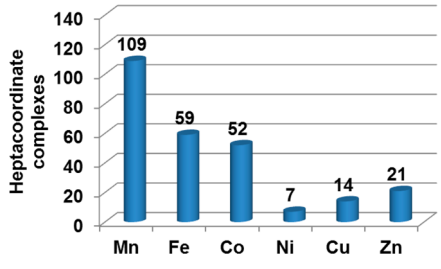


**Figure 1.** Number of heptacoordinate complexes found in the Cambridge Structural Database (CSD).

**Received:** July 31, 2014
**Published:** November 21, 2014

   dx.doi.org/10.1021/ic501869y | *Inorg. Chem.* 2014, 53, 12859−12869

coordinate complexes along the transition metal series can be explained in part by the decreased ionic radii of the metal ions. However, seven-coordination appears to be more frequent for Cu and Zn than for Ni. The coordination chemistry of Ni is dominated by the divalent oxidation state, which indicates that seven-coordinated complexes are particularly rare along the first-row transition metal series for the $d^8$ configuration.

In the late 1980s, two different groups reported almost simultaneously stability constants of different divalent and trivalent metal complexes with the ligand 1,4,10-trioxa-7,13-diazacyclopentadecane-*N*,*N*′-diacetic acid ($H_2L^1$, Chart 1).[6−8]

**Chart 1. Structures of Ligands Mentioned in This Work**

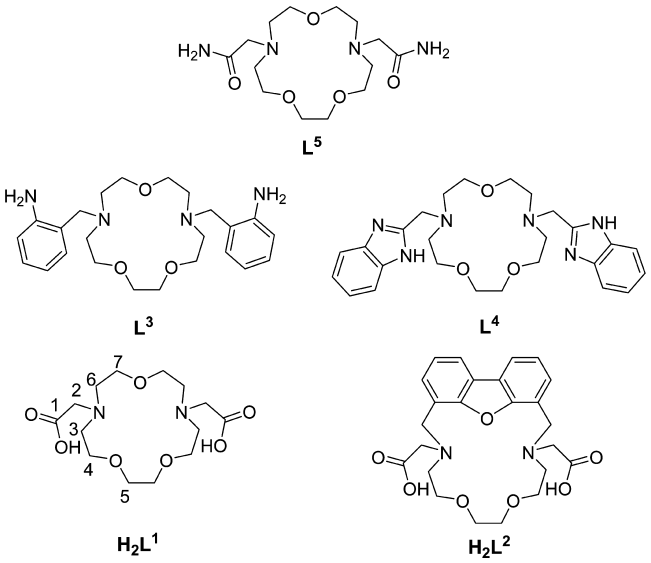


The stability constants determined by Delgado et al. for the first-row transition metal ions showed an interesting trend that contradicts the Irving−Williams order (Figure 2). The Irving−

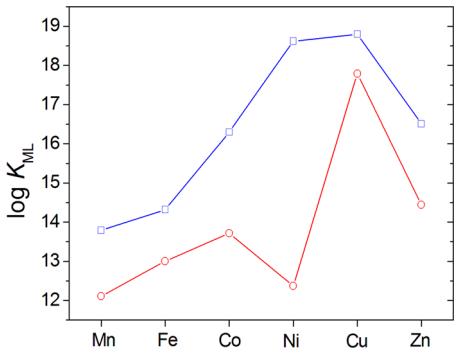


**Figure 2.** Stability constants of $[M(L^1)]$ (red circles) and $[M(edta)]^{2-}$ (blue squares) complexes.

Williams order of stability ($Mn^{2+} < Fe^{2+} < Co^{2+} < Ni^{2+} < Cu^{2+} > Zn^{2+}$) holds for many high-spin octahedral complexes, and it is a consequence of the increasing ligand-field stabilization energy on proceeding to the right across the first-row transition metal series from $Mn^{2+}$ to $Ni^{2+}$ and the stabilization of octahedral complexes with $Cu^{2+}$ through tetragonal Jahn−Teller elongation. This is the case, for instance, for $[M(edta)]^{2-}$ complexes, which show stabilities in agreement with the Irving−Williams series (Figure 2).[9] However, the Irving−Williams order does not hold for metal complexes with different coordination numbers and/or geometries. Delgado et al. did notice the uncommon stability trend of $[M(L^1)]$ complexes, and concluded that the metal coordination environment was not octahedral. Soon after, the X-ray structure of the $[Cu(L^1)]\cdot 2H_2O$ was reported, showing that the metal coordination environment is distorted pentagonal bipyramidal.[10] More recent studies reported by Delgado showed that the $[Ni(L^2)]$ complex is six-coordinated, with one of the ether oxygen atoms of the crown moiety not being involved in the coordination to the metal ion (Chart 1).[11]

In previous works we have demonstrated that receptors *N*,*N*′-bis(2-aminobenzyl)-1,4,10-trioxa-7,13-diazacyclopentadecane ($L^3$) and *N*,*N*′-bis(benzimidazol-2ylmethyl)-1,4,10-trioxa-7,13-diazacyclopentadecane ($L^4$) yield mononuclear divalent first-row transition-metal-ion complexes with pentagonal bipyramidal geometry (M = Mn, Co, Cu, Zn, Chart 1).[12−16] In these complexes the trioxadiaza macrocyclic moiety provides the five donor atoms of the equatorial plane, while the donor atoms of the pendant arms occupy the apical positions. The $[NiL^3]^{2+}$ complex shows a severely distorted pentagonal bipyramidal coordination,[12] while in $[NiL^4]^{2+}$ the metal ion is only six-coordinate in a distorted octahedral coordination environment.[13] The structural differences observed for the $Ni^{2+}$ analogues have been suggested to be the result of the Jahn−Teller effect operating in pentagonal bipyramidal $Ni^{2+}$ complexes. In recent reports the six-coordinate closely related derivative $[NiL^5]^{2+}$ was proposed as candidate for a new class of contrast agents for magnetic resonance imaging based on the chemical exchange saturation transfer effect (CEST).[17]

In light of the studies performed on the complexes of $L^3$ and $L^4$, it is likely that the $[M(L^1)]$ complexes (M = Mn, Co, Cu, and Zn) present seven-coordinated structures with pentagonal bipyramidal coordination environments,[18] while the structure of the $Ni^{2+}$ analogue is more difficult to anticipate. To address these fundamental questions, in this work we investigate the structure of the $[M(L^1)]$ (M = Co, Ni, Cu, or Zn) complexes by using a combination of experimental and theoretical techniques. The structure of these complexes in solution was investigated by using NMR and EPR spectroscopies, while DFT calculations were used to gain insight into their electronic structure. The X-ray structures of the complexes with $Co^{2+}$, $Ni^{2+}$, and $Cu^{2+}$ are also reported. The results obtained from this study were used to provide a justification of the different relative abundances of seven-coordinated complexes along the first-row transition metal series. An understanding of the factors that favor the formation of seven-coordinate complexes will be beneficial for the design of ligands with high selectivity for specific metal ions or the stabilization of unusual oxidation states.

## EXPERIMENTAL SECTION

**General Methods.** Elemental analyses were carried out on a Carlo Erba 1108 elemental analyzer. ESI-TOF mass spectra were recorded using a LC-Q-q-TOF Applied Biosystems QSTAR Elite spectrometer in the positive mode. UV−vis spectra were recorded on PerkinElmer Lambda 900, PerkinElmer Lambda 45, or Shimadzu UV3100 spectrophotometer in 1.0 cm path quartz cells. IR spectra were recorded on a Bruker Vector 22 instrument with an ATR accessory. $^1H$ and $^{13}C$ NMR spectra were recorded at 25 °C on a Bruker Avance 500 MHz spectrometer. For measurements in $D_2O$, *tert*-butyl alcohol was used as an internal standard with the methyl signal calibrated at $\delta = 1.2$ ($^1H$) and 31.2 ppm ($^{13}C$). Spectral assignments were based in part on two-dimensional COSY, HSQC, and HMBC experiments. EPR spectra of the copper(II) complex were measured on a Bruker EMX


dx.doi.org/10.1021/ic501869y | *Inorg. Chem.* 2014, 53, 12859−12869

300 spectrometer operating in the X-band that was equipped with a continuous-flow cryostat for liquid nitrogen. Measurements were recorded at 298 K and in frozen solutions (90 K) using different solvents (the concentration of the complex was 1 mM, pH 7.0). A microwave power of 2.0 mW was used, while the modulation amplitude was 1.0 mT and the frequency ($\nu$) 9.51 GHz. Selected EPR spectra were simulated with the SpinCount[19] software to determine the relevant parameters. Preparative medium pressure liquid chromatography was carried out using a CombiFlash Rf system using neutral $Al_2O_3$ RediSepRf columns (column size 48 g, particle size 40−63 $\mu$m, pore size 60 Å). All chemicals were purchased from commercial sources and used without further purification, unless otherwise stated.

**Di-*tert*-butyl 2,2′-(1,4,10-trioxa-7,13-diazacyclopentadecane-7,13-diyl)diacetate (1).** A mixture of 1,4,10-trioxa-7,13-diazacyclopentadecane (1.00 g, 4.58 mmol) and $Na_2CO_3$ (3.88 g, 36.6 mmol) in acetonitrile (150 mL) was stirred for 30 min, and then *tert*-butyl-2-bromoacetate (1.88 g, 9.62 mmol) and a catalytic amount of KI were added. The mixture was stirred at 45 °C under an inert atmosphere (Ar) for a period of 120 h, and then the excess $Na_2CO_3$ was filtered off. The filtrate was concentrated to dryness, and the yellow oil was extracted with a 1:3 mixture of $H_2O$ and $CH_2Cl_2$ (300 mL). The organic phase was evaporated to dryness to give an oily residue that was purified by preparative medium pressure liquid chromatography (neutral $Al_2O_3$ with a $CH_2Cl_2$/MeOH mixture as the eluent; gradient 0−10%) to give **1** (1.91 g) as a yellow oil. Yield: 68%. Anal. Calcd for $C_{22}H_{42}N_2O_7{\cdot}2CH_2Cl_2$: C 46.76, H 7.52, N 4.54%. Found: C 46.54, H 7.25, N 4.36%. MS (ESI$^+$, MeOH:$CH_3CN$:$H_2O$ 9:1:1): $m/z$ 447 ($[C_{22}H_{43}N_2O_7]^+$). IR (ATR): $\nu$ 1730 cm$^{-1}$ (C═O). $^1$H NMR ($CDCl_3$, 500 MHz, 25 °C, TMS): $\delta$ 3.63 (m, 12 H), 3.50 (m, 4 H), 3.05 (m, 8 H), 1.46 ppm (s, 18 H). $^{13}$C NMR ($CDCl_3$, 125.8 MHz, 25 °C, TMS): $\delta$ 170.0, 70.4, 69.4, 68.7, 56.8, 54.5, 54.0, 28.2 ppm.

**1,4,10-Trioxa-7,13-diazacyclopentadecane-7,13-diacetic Acid ($H_2L^1$).** The di-*tert*-butyl ester **1** (1.91 g, 3.10 mmol) was dissolved in a 1:1 mixture of dichloromethane and trifluoroacetic acid (30 mL). The mixture was heated to reflux with stirring for 24 h, and then the solvents were removed in a rotary evaporator to give a brown oil. This was dissolved in $H_2O$ (10 mL), and the solvent was evaporated. This process was repeated twice, and then three times with diethyl ether. The oily residue was dried under vacuum to give 1.48 g of the expected compound. Yield: 85%. Anal. Calcd for $C_{14}H_{26}N_2O_7{\cdot}2CF_3COOH$: C 38.44, H 5.02, N 4.98%. Found: C 38.20, H 5.22, N 4.76%. MS (ESI$^+$, MeOH:$CH_3CN$:$H_2O$ 9:1:1): $m/z$ 335 ($[C_{14}H_{27}N_2O_7]^+$). IR (ATR): $\nu$ 1731 and 1667 cm$^{-1}$ (C═O). $^1$H NMR ($D_2O$, pD 7.0, 500 MHz, 25 °C, TMS): $\delta$ 4.09 (m, 4 H), 3.87 (m, 8 H), 3.72 (m, 4 H), 3.62 ppm (m, 8 H). $^{13}$C NMR ($D_2O$, pD 7.0, 125.8 MHz, 25 °C, TMS): $\delta$ 170.5, 71.4, 64.9, 64.6, 56.7, 56.3, 55.4 ppm.

**General Procedure for the Preparation of [ML]·x$H_2O$ Complexes (M = Co, Ni, Cu, or Zn).** A solution of $H_2L^1{\cdot}2CF_3COOH$ (0.100 g, 0.178 mmol), triethylamine (0.072 g, 0.711 mmol), and $M(OTf)_2$ (0.178 mmol, M = Co, Ni, Cu, or Zn) in a mixture of 2-propanol and MeOH (9:1, 10 mL) was heated to reflux for 4 h. The reaction was allowed to cool down to room temperature and then concentrated to dryness. The addition of 5 mL of THF resulted in the formation of a precipitate, which was isolated by filtration. The solid was then suspended in 10 mL of THF and stirred at room temperature for 24 h. The solid was isolated by filtration, washed with THF and diethyl ether, and dried under vacuum.

**[CoL$^1$]·3$H_2O$.** Characterization details follow: light pink solid. Yield 0.060 g, 76%. UV−vis ($H_2O$, pH = 7.0): $\lambda_{max}$ = 493 nm ($\varepsilon$ 10 M$^{-1}$ cm$^{-1}$), $\lambda_{max}$ = 785 nm ($\varepsilon$ 4 M$^{-1}$ cm$^{-1}$). Anal. Calcd for $C_{14}H_{24}CoN_2O_7{\cdot}3H_2O$: C, 37.76; H, 6.79; N, 6.29%. Found: C, 37.61; H, 6.37; N, 6.16%. HR-MS (ESI$^+$, MeOH:$CH_3CN$:$H_2O$ 9:1:1): $m/z$ 414.0814; calcd for $[C_{14}H_{24}CoN_2NaO_7]^+$ 414.0807. IR (ATR, cm$^{-1}$): $\nu$ 1589 (C═O).

**[NiL$^1$]·3$H_2O$.** Characterization details follow: light green solid. Yield 0.056 g, 71%. UV−vis ($H_2O$, pH = 7.0): $\lambda_{max}$ = 409 nm ($\varepsilon$ 21 M$^{-1}$ cm$^{-1}$), $\lambda_{max}$ = 664 nm ($\varepsilon$ 8 M$^{-1}$ cm$^{-1}$), $\lambda_{max}$ = 1347 nm ($\varepsilon$ 12 M$^{-1}$ cm$^{-1}$). Anal. Calcd for $C_{14}H_{24}N_2NiO_7{\cdot}3H_2O$: C, 37.78; H, 6.79; N, 6.29%. Found: C, 37.83; H, 6.78; N, 5.98%. HR-MS (ESI$^+$, MeOH:$CH_3CN$:$H_2O$ 9:1:1): $m/z$ 413.0816; calcd for $[C_{14}H_{24}N_2NaNiO_7]^+$ 413.0829. IR (ATR, cm$^{-1}$): $\nu$ 1593 (C═O).

**[CuL$^1$]·$H_2O$.** Characterization details follow: light blue solid. Yield 0.055 g, 75%. UV−vis ($H_2O$, pH = 7.0): $\lambda_{max}$ = 820 nm ($\varepsilon$ 84 M$^{-1}$ cm$^{-1}$). Anal. Calcd for $C_{14}H_{24}CuN_2O_7{\cdot}H_2O$: C, 40.62; H, 6.33; N, 6.77%. Found: C, 40.84; H, 6.19; N, 6.50%. HR-MS (ESI$^+$, MeOH:$CH_3CN$:$H_2O$ 9:1:1): $m/z$ 418.0782; calcd for $[C_{14}H_{24}CuN_2NaO_7]^+$ 418.0771. IR (ATR, cm$^{-1}$): $\nu$ 1620 (C═O).

**[ZnL$^1$]·3$H_2O$.** Characterization details follow: white solid. Yield 0.065 g, 81%. Anal. Calcd for $C_{14}H_{24}N_2O_7Zn{\cdot}3H_2O$: C, 37.22; H, 6.69; N, 6.20%. Found: C, 37.23; H, 6.56; N, 5.95%. HR-MS (ESI$^+$, MeOH:$CH_3CN$:$H_2O$ 9:1:1): $m/z$ 419.0760; calcd for $[C_{14}H_{24}N_2NaO_7Zn]^+$ 419.0767. IR (ATR, cm$^{-1}$): $\nu$ 1593 (C═O). $^{13}$C NMR ($D_2O$, pD 7.0, 125.8 MHz, 25 °C, TMS): $\delta$ 180.5, 69.9, 67.1, 65.1, 59.3, 56.7, 55.4 ppm.

**X-ray Crystal Structures.** Single crystals were obtained by slow diffusion of diethyl ether into solutions of the complexes in methanol at room temperature. Three-dimensional X-ray data were collected on a Bruker CCD SMART1000 diffractometer. All three data sets were corrected for Lorentz and polarization effects and for absorption by semiempirical methods[20] based on symmetry-equivalent reflections. Complex scattering factors were taken from the program SHELX97[21] running under the WinGX program system[22] as implemented on a Pentium computer. All the structures were solved by Patterson methods (SHELXS97 for [NiL$^1$]·2$H_2O$ and DIRDIF 2008 for [CoL$^1$] and [CuL$^1$])[21,23] and refined[21] by full-matrix least-squares on $F^2$. All three compounds crystallize in noncentrosymmetric space groups, and therefore, crystal data were refined using the TWIN and BASF instructions of SHELXL97;[21] the Flack[24] parameters obtained are included in Table 1. The crystals of the Ni complex belong to an enantiomorphic space group. This fact, together with the presence of a racemic mixture in the crystal lattice, led us to check the possibility of a solution in a centrosymmetric space group. However, the analysis performed with the ADDSYM program[25] does not provide any evidence of a symmetry center. Hydrogen atoms were included in calculated positions and refined in riding mode in all cases, except those of the water molecules present in [NiL$^1$]·2$H_2O$, which were located in a difference electron-density map and the OH and HH distances restrained. Refinement converged with anisotropic displacement parameters for all non-hydrogen atoms. Crystal data and details on data collection and refinement are summarized in Table 1.

**Computational Methods.** Full geometry optimizations of the [ML$^1$] and $[M(H_2O)_6]^{2+}$ systems (M = Co, Ni, Cu, or Zn) were performed both in the gas phase and in aqueous solution employing DFT within the hybrid meta-GGA approximation with the TPSSh exchange-correlation functional[26] and the Gaussian 09 package (Revision B.01).[27] In these calculations we used the standard Ahlrichs' valence triple-$\xi$ basis sets including polarization functions (TZVP).[28] No symmetry constraints have been imposed during the optimizations. The $Co^{2+}$ and $Ni^{2+}$ complexes were modeled in their high-spin configurations (Co, $S = {}^3/_2$; Ni, $S = 1$). Geometry optimizations of the Co, Ni, and Cu complexes were performed by using an unrestricted model,[29] and therefore, spin contamination was assessed by comparison of the expected difference between $S(S + 1)$ for the assigned spin state and the actual value of $\langle S^2 \rangle$.[30] The results indicate that spin contamination is negligible for all complexes investigated. The stationary points found on the potential energy surfaces as a result of geometry optimizations were tested to represent energy minima rather than saddle points via frequency analysis. The default values for the integration grid (75 radial shells and 302 angular points) and the SCF energy convergence criteria ($10^{-8}$) were used in all calculations. Throughout this work solvent effects were included by using the polarizable continuum model (PCM), in which the solute cavity is built as an envelope of spheres centered on atoms or atomic groups with appropriate radii. In particular, we used the integral equation formalism (IEFPCM) variant as implemented in Gaussian 09.[31] Basis Set Superposition Errors (BSSEs), which represent an undesirable consequence of using finite basis sets that leads to an overestimation of


dx.doi.org/10.1021/ic501869y | Inorg. Chem. 2014, 53, 12859−12869

**Table 1. Crystal Data and Refinement Details of the Complexes**

| | $[CoL^1]$ | $[NiL^1]\cdot 2H_2O$ | $[CuL^1]$ |
|---|---|---|---|
| formula | $C_{14}H_{24}CoN_2O_7$ | $C_{14}H_{28}N_2NiO_9$ | $C_{14}H_{24}CuN_2O_7$ |
| MW | 391.28 | 427.09 | 395.89 |
| cryst syst | monoclinic | tetragonal | monoclinic |
| space group | $P12_11$ | $P4_32_12$ | $P2_1$ |
| $T$/K | 100(2) | 100(2) | 100(2) |
| $a$/Å | 7.0823(17) | 7.088(3) | 7.1445(17) |
| $b$/Å | 12.093(3) | 7.088(3) | 12.036(3) |
| $c$/Å | 9.591(2) | 34.725(16) | 9.538(2) |
| $\alpha$/deg | 90 | 90 | 90 |
| $\beta$/deg | 108.514(3) | 90 | 108.082(3) |
| $\gamma$/deg | 90 | 90 | 90 |
| $V$/Å$^3$ | 778.9(3) | 1744.6(17) | 779.7(3) |
| $F(000)$ | 410 | 904 | 414 |
| $Z$ | 2 | 4 | 2 |
| $\lambda$, Å (Mo K$\alpha$) | 0.710 73 | 0.710 73 | 0.710 73 |
| $D_{calcd}$/g cm$^{-3}$ | 1.668 | 1.626 | 1.686 |
| $\mu$/mm$^{-1}$ | 1.143 | 1.165 | 1.442 |
| $\theta$ range/deg | 2.24−26.37 | 2.346−26.221 | 2.25−25.68 |
| $R_{int}$ | 0.0312 | 0.0643 | 0.0205 |
| reflns measured | 3158 | 15 172 | 2919 |
| unique reflns | 3158 | 1759 | 2919 |
| reflns obsd | 3046 | 1625 | 2678 |
| Flack param | 0.27(2) | 0.55(2) | 0.47(3) |
| GOF on $F^2$ | 1.043 | 1.075 | 1.061 |
| R1[a] | 0.0400 | 0.0279 | 0.0542 |
| wR2 (all data)[b] | 0.1062 | 0.0602 | 0.1488 |
| largest differences peak and hole/e Å$^{-3}$ | 0.768/−0.436 | 0.261/−0.378 | 1.240/−0.430 |

[a] $R1 = \sum||F_o| - |F_c||/\sum|F_o|$. [b] $wR2 = \{\sum[w(|F_o|^2 - |F_c|^2)^2]/\sum[w(F_o^4)]\}^{1/2}$.

the binding energy, were calculated using the standard Counterpoise method[32] with calculations performed in the gas phase.[33] The NMR shielding tensors of the $[ZnL^1]$ system were calculated in aqueous solution (IEFPCM) at the TPSSh/TSVP level by using the GIAO method.[34] For $^{13}C$ NMR chemical shift calculation purposes the NMR shielding tensors of TMS were calculated at the same level.

The calculation of the $g$- and $A$-tensors of the $[CuL^1]$ complex was carried out using the ORCA program package (Version 3.0.1)[35] and the methodology developed by Neese.[36] The TPSSh functional was used in these calculations, as it has been shown that it is at least as accurate as or better than the B3LYP functional and significantly superior to the nonhybrid TPSS variant, for the prediction of hyperfine structure.[37] For comparative purposes, some calculations were also performed using the BHLYP functional.[38] The geometry of the $[CuL^1]$ complex optimized with the Gaussian code as described above was employed. We have taken the center of the electronic charge as the origin for the calculation of the $g$-tensor, which is a gauge dependent property. The different contributions to the $g$-tensor are the relativistic mass correction, the diamagnetic spin−orbit term, and the paramagnetic spin−orbit term. The $A$-tensor is calculated as a sum of three terms: (a) the isotropic Fermi contact (FC) term, (b) the spin-dipolar (SD) term, and (c) the spin−orbit coupling (SOC) term. The spin−orbit contributions to the hyperfine coupling constants and $g$ values were computed via the spin−orbit mean field approach (SOMF) using the one-center approximation to the exchange term (SOMF(1X)).[39] The basis sets used for the EPR parameter calculations were the core properties (CP) basis set for Cu developed by Neese,[40] and the Default-Basis 5 basis set for all other atoms. The latter basis is based on the Ahlrichs TZV basis sets,[41] and includes polarization and diffuse functions from the 6-311++G(2d,2p) basis set.[42] The CP basis set contains additional steep primitives at the core region, improving calculated core property values, such as the $A$-tensor. The RI-JK approximation[43] was used to speed up calculations of the EPR parameters using the def2-TZV[44] auxiliary basis set as constructed automatically by ORCA. The convergence tolerances and integration accuracies of the calculations were increased from the defaults using the available TightSCF and Grid5 options. Solvent effects (water) were taking into account by using the COSMO solvation model as implemented in ORCA.[45]

## RESULTS AND DISCUSSION

**Synthesis and Characterization of the Ligand and Its Metal Complexes.** A synthesis of $H_2L^1$ involving the alkylation of 1,4,10-trioxa-7,13-diazacyclopentadecane with potassium chloroacetate in aqueous solution has been reported, but the yield of the reaction was not provided.[6] The ligand $H_2L^1$ was also obtained in 41% by Chang et al.[7] by $N$-alkylation of 1,4,10-trioxa-7,13-diazacyclopentadecane with ethyl bromoacetate followed by hydrolysis of the ethyl ester intermediate. $N$-Alkylation reactions of polyamines with ethyl bromoacetate often proceed with rather low yields due to the formation of lactams and other amides resulting from intermolecular reactions, while analogous reactions using *tert*-butyl bromoacetate usually give higher yields.[46] Thus, we prepared $H_2L^1$ by reaction of 1,4,10-trioxa-7,13-diazacyclopentadecane with *tert*-butyl bromoacetate using $Na_2CO_3$ as a base, followed by deprotection of the *tert*-butyl ester groups with trifluoroacetic acid. The ligand was isolated as the trifluoroacetate salt in 58% overall yield, which represents a 17% improvement with respect to the synthesis reported by Chang et al.[7]

The $H_2L^1$ ligand was derivatized to form the charge-neutral $[ML^1]$ complexes (M = Co, Ni, Cu, or Zn), which were obtained in 71−81% yield by reaction of the ligand with equimolar amounts of the corresponding metal triflate in the presence of triethylamine. The mass spectra of the complexes (positive ion electrospray ionization, ESI$^+$) show intense peaks due to the $[M(L^1 + Na)]^+$ entities, which confirm the formation of the expected complexes (Figures S2−S5, Supporting Information).

**X-ray Crystal Structures.** The solid-state structures of the Co, Ni, and Cu complexes were determined by single-crystal X-ray diffraction analyses. Crystals contain the expected neutral $[ML^1]$ complexes, and, in the case of the Ni complex, water molecules involved in hydrogen-bonding interaction with the uncoordinated oxygen atoms of the acetate groups. $[CuL^1]$ crystallizes in the monoclinic $P2_1$ space group, while the structure of $[CuL^1]\cdot 2H_2O$ reported previously was solved in the tetragonal $P4_3$ space group.[10] However, the bond distances and angles of the $Cu^{2+}$ coordination environment remain very similar in the two structures. Table 2 summarizes selected bond lengths and angles of the metal coordination environments, while the structures of the complexes are depicted in Figure 3.

The complexes of $Co^{2+}$ and $Cu^{2+}$ present a slightly distorted $C_2$ symmetry in the solid state, with the symmetry axis passing through O5 and the metal ion. For $[NiL^1]$ the $C_2$ symmetry is crystallographically imposed. The macrocyclic ligand is arranged in an *anti* conformation, with the two pendant arms placed on opposite sides of the macrocyclic fragment. The metal ions are placed inside the macrocyclic cavity with the donor atoms of the pendant arms coordinating apically.

The most common coordination polyhedron for seven-coordinate complexes of transition metal ions is the pentagonal bipyramid, followed by the capped trigonal prism and the capped octahedron.[1] The metal coordination environments in


dx.doi.org/10.1021/ic501869y | Inorg. Chem. 2014, 53, 12859−12869

**Table 2. Bond Distances (Å) and Angles (deg) of the Metal Coordination Environments in [ML$^1$] Complexes (M = Co, Ni, or Cu)[a]**

| | [CoL$^1$] | [CuL$^1$] | | [NiL$^1$] |
|---|---|---|---|---|
| M1−O6 | 2.025(3) | 1.945(5) | Ni1−O1 | 1.985(2) |
| M1−O1 | 2.030(3) | 1.906(4) | Ni1−O3 | 2.544(3) |
| M1−N2 | 2.199(3) | 2.137(5) | Ni1−O4 | 2.051(3) |
| M1−N1 | 2.242(3) | 2.078(5) | Ni1−N2 | 2.133(3) |
| M1−O5 | 2.297(3) | 2.513(5) | O1−Ni1−O1$^i$ | 172.09(14) |
| M1−O4 | 2.312(2) | 2.517(4) | O1−Ni1−O4 | 93.95(7) |
| M1−O3 | 2.339(3) | 2.482(4) | O1−Ni1−N2 | 83.29(9) |
| O6−M1−O1 | 176.10(11) | 176.6(2) | O1$^i$−Ni1−N2 | 98.30(9) |
| O6−M1−N2 | 81.35(10) | 82.90(18) | O4−Ni1−N2 | 78.54(7) |
| O1−M1−N2 | 96.00(10) | 98.69(18) | N2−Ni1−N2$^i$ | 157.09(14) |
| O6−M1−N1 | 104.42(10) | 94.35(19) | O1−Ni1−O3 | 94.30(8) |
| O1−M1−N1 | 79.36(10) | 85.7(2) | O1$^i$−Ni1−O3 | 78.86(8) |
| O6−M1−O5 | 85.82(11) | 101.52(18) | O4−Ni1−O3 | 149.00(5) |
| O1−M1−O5 | 96.18(11) | 81.73(16) | N2−Ni1−O3 | 72.84(8) |
| N2−M1−O5 | 73.12(10) | 78.20(16) | N2$^i$−Ni1-O3 | 129.46(8) |
| N1−M1−O5 | 74.89(10) | 73.52(18) | O3−Ni1−O3$^i$ | 62.01(10) |
| O6−M1−O4 | 93.16(10) | 100.14(17) | | |
| O1−M1−O4 | 83.39(10) | 77.57(16) | | |
| N2−M1−O4 | 75.73(10) | 73.33(17) | | |
| O6−M1−O3 | 81.49(9) | 80.89(16) | | |
| O1−M1−O3 | 98.84(10) | 95.86(16) | | |
| N1−M1−O3 | 73.67(10) | 77.02(17) | | |
| O4−M1−O3 | 68.39(8) | 64.54(14) | | |

[a]Superscripts denote symmetry transformations used to generate equivalent atoms: i = y, x, −z.

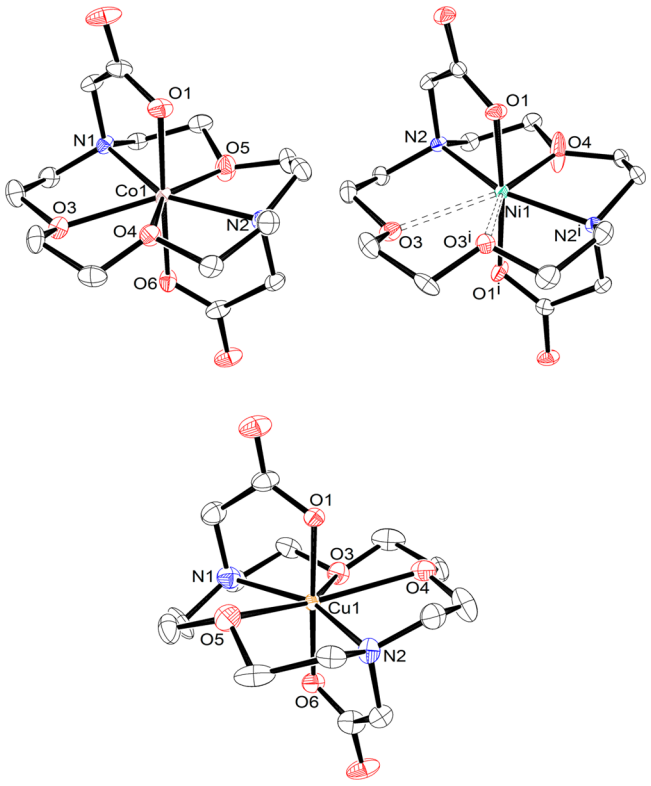


**Figure 3.** X-ray crystal structures of the [Co(L$^1$)], [Ni(L$^1$)], and [Cu(L$^1$)] complexes. Hydrogen atoms are omitted for simplicity. The ORTEP plots are at the 30% probability level.

[CoL$^1$], [NiL$^1$], and [CuL$^1$] can be described as pentagonal bipyramidal, where the equatorial plane is defined by the five donor atoms of the macrocycle. This is confirmed by performing continuous shape measures with the assistance of the SHAPE program.[47,48] The analysis of the coordination polyhedra provides shape measures for pentagonal bipyramidal coordination of 1.74 ([CoL$^1$]), 1.82 ([NiL$^1$]), and 2.99 ([CuL$^1$]), while capped octahedron gives shape measures of 4.43 (Co), 4.95 (Ni), and 4.97 (Cu), and capped trigonal prism yields 3.14 (Co), 3.60 (Ni), and 4.17 (Cu) (the shape measure $S$(A) = 0 for a structure fully coincident in shape with the reference polyhedron and the maximum allowed value of $S$(A) is 100).

The O6−M1−O1 angles in the [CoL$^1$] and [CuL$^1$] complexes deviate by ca. 4° from the ideal value for a pentagonal bipyramid (180°), while the O1−Ni1−O1$^i$ angle observed for [NiL$^1$] of 172.09(14)° deviates slightly more from 180°. Angles D1M1D2, where D1 and D2 represent adjacent donor atoms of the equatorial plane, are close to the ideal value of 72° (Table 2), while the vectors defined by the metal ion and the axial donors O1 and O6 form angles that are relatively close to 90° with the vectors containing the metal ion and the equatorial donor atoms, as expected for a pentagonal bipyramidal coordination.

The pentagonal bipyramidal coordination polyhedra are axially compressed, as the apical bonds are considerably shorter than the equatorial bonds. The oxygen donor atoms of acetate groups provide the strongest interaction with the metal ion, while for the complexes with $Co^{2+}$ and $Cu^{2+}$ the oxygen atoms of the crown moiety provide the longest M−donor distances. Moreover, the three M−$O_{crown}$ distances observed for the complexes of $Co^{2+}$ and $Cu^{2+}$ are very similar. The structure of the complex of $Ni^{2+}$ differs from those of $Co^{2+}$ and $Cu^{2+}$, as it shows a very short Ni−$O_{crown}$ distance [Ni1−O4 2.051(3) Å] and two long ones [Ni1−O3 and Ni1−O3$^i$ 2.544(3) Å].

**Structure in Solution.** Geometry optimizations performed using DFT calculations in aqueous solution at the TPSSh/TZVP level on the [CoL$^1$] and [CuL$^1$] complexes provide molecular structures in reasonably good agreement with the corresponding X-ray structures, with average unsigned deviations of 1.3% and 2.1%, respectively. The calculated bond distances of the metal coordination environment are compared to the experimental distances in Table S1 (Supporting Information). The calculated geometries present slightly distorted $C_2$ symmetries, in agreement with the solid-state structures. A similar structure is obtained for the [ZnL$^1$] complex. The situation is however different for the [NiL$^1$] complex. Indeed, geometry optimizations of this complex using the solid-state structure as input geometry gave a molecular structure with a very distorted geometry in which the distances to the two nitrogen atoms of the ligand and the oxygen atoms O3 and O4 differ significantly (Figure 4). Furthermore, a careful investigation of the conformational space for this complex provides two additional energy minima. These three energy minima present very different bond distances of the metal coordination environment, and are labeled as I, II, and III (Figure 4). Form I presents a short Ni−O5 distance (2.093 Å), and long Ni−O3 and Ni−O4 distances (2.404 and 2.825 Å, respectively). In the second form (II) O5 is not bound to the metal ion (Ni···O5 3.373 Å), with the metal coordination environment being best described as distorted octahedral. The third energy minimum (III) shows a long Ni−O5 distance (2.669 Å) and short Ni−O4 and Ni−O3 bonds (2.138 and


dx.doi.org/10.1021/ic501869y | Inorg. Chem. 2014, 53, 12859−12869

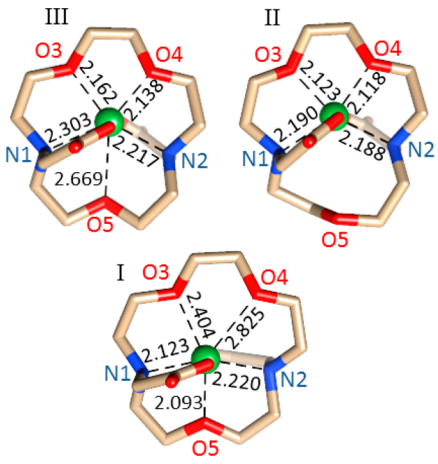


**Figure 4.** Views of the three energy minima obtained with DFT calculations (TPSSh/TZVP) in aqueous solution for the [NiL$^1$] complex. Bond distances of the metal coordination environment involving donor atoms of the crown moiety are given in Å. Hydrogen atoms are omitted for simplicity.

2.162 Å, respectively). A similar six-coordinate complex was observed for [NiL$^4$]$^{2+}$ in the solid state.[13] It is noteworthy that the distances to the donor atoms of the carboxylate groups are very similar for the three structures (2.005 ± 0.013 Å).

The potential energy surface of [NiL$^1$] was investigated by performing relaxed potential energy scans along the Ni−O5 coordinate (Figure 5). Our results indeed confirmed the

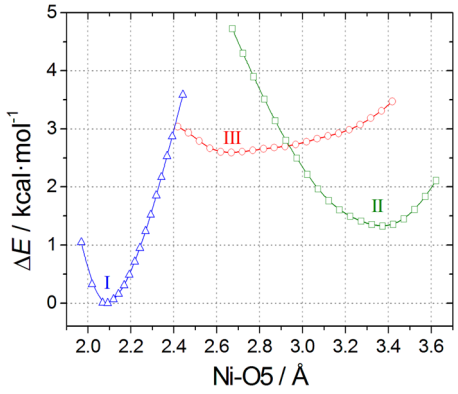


**Figure 5.** Relaxed potential energy surface scan calculated for [NiL$^1$] in aqueous solution at the TPSSh/TZVP level as a function of the Ni−O5 distance.

presence of three different energy minima. The corresponding potential energy curves show evident crossings, which are characteristic of a metal complex suffering a Jahn−Teller effect.[49] According to our calculations the structure labeled as I is more stable than II and III, with the zero point energy corrected relative energies of forms II and III with respect to I amounting to 1.69 and 2.62 kcal mol$^{-1}$. Thus, the minimum energy geometry obtained with DFT calculations in aqueous solution (form I) corresponds to the structure found experimentally in the solid state. Simple considerations using ligand-field theory show that the lengthening of the Ni−O3 and Ni−O4 distances and concomitant shortening of the Ni−O5 bond increases the energy gap between the $d_{x^2-y^2}$ and $d_{xy}$ orbitals, which are strictly degenerated in $D_{5h}$ symmetry (Figure 6).

The $^1$H and $^{13}$C NMR spectra of the diamagnetic [ZnL$^1$] complex were obtained in $D_2O$ solution at pD = 7.0 (Figure S8, Supporting Information), and partially assigned on the basis of two-dimensional COSY, HSQC, and HMBC experiments. The $^{13}$C NMR spectrum exhibits 7 signals for the 14 carbon nuclei of the ligand backbone, pointing to an effective $C_2$ symmetry of the complex in solution. The H2 methylene protons show an AB pattern ($^2J$ = 18.6 Hz, see Chart 1 for labeling) in which the equatorial protons are deshielded due to the polarization of the C−H bond by the electric field generated by the cation charge. The axial and equatorial protons of the macrocyclic fragment are magnetically nonequivalent, which indicates that the interconversion between $\delta$ and $\lambda$ conformations of the five-membered chelate rings formed upon coordination of the macrocyclic moiety is slow at the NMR time-scale. This points to a relatively rigid structure of the crown moiety in solution that is compatible with a seven-coordinated complex. The specific assignment of several pairs of NMR signals (3−6, 4−7) was not possible on the basis of the 2D NMR spectra. Thus, the $^{13}$C NMR shifts were calculated using the GIAO method, which has been shown to provide good estimates of $^{13}$C NMR shifts for $Zn^{2+}$ complexes.[50] The calculated shifts show an excellent agreement with the corresponding experimental values (Table 3), which confirms that the [ZnL$^1$] complex adopts a seven-coordinated geometry in aqueous solution. The assignment of the carbon signals allowed a full assignment of the $^1$H NMR spectrum from the cross-peaks observed in the HSQC experiment.

The vis−NIR spectra of [CuL$^1$] were obtained in aqueous solution in a wide range of pH (2.8−9.1) without significant changes of the bands. The spectra show a broad absorption band due to the copper d−d transitions centered at $\lambda$ = 820 nm ($\varepsilon$ = 83.7 M$^{-1}$ cm$^{-1}$) that tails into the low-energy region of the spectrum with shoulders at 960 and 1100 nm in the NIR region. The position and intensity of the vis−NIR bands rules out regular octahedral or tetragonal geometries.[51] However, it is difficult to infer structural features from electronic spectra of copper(II) complexes only, as their stereochemistries vary over an appreciable range of distortion within a given coordination number, which is known as the plasticity effect.[52] In other solvents, such as EtOH or DMF, the bands maintain the same appearance but shift to the blue ($\lambda_{max}$ = 790 nm for ethanol, and 750 nm for DMF, see Figure S9, Supporting Information).

To assist the structural characterization of the [CuL$^1$] complex in solution, X-band EPR spectra were obtained in different solvents at 90 and 298 K. Figure 7 shows the spectrum of the complex in water:DMSO (9:1) and its corresponding simulation. The spectra recorded in all solvents (frozen water:glycerol (9:1 v/v), water:DMSO (9:1), DMF, and EtOH solutions) are rather similar, differing only in resolution. The EPR parameters obtained by simulation[19] of the spectra of complexes are compiled in Table 4.

Three different values of $g$ were obtained for the [CuL$^1$] complex, with $g_z > g_y > g_x$ and $g_x \geq 2.03$, revealing a very distorted structure. The magnitude of the $Cu^{2+}$ hyperfine coupling constant ($A_z$) in the complex was found to be very low in comparison to those of copper(II) complexes with $d_{xy}$ or $d_{x^2-y^2}$ ground states, which is indicative of a low symmetry. In fact, such large reduction in copper(II) hyperfine coupling is explained in terms of a mixed $d_{x^2-y^2}/d_{z^2}$ ground state and delocalization of unpaired spin density onto the ligands. Since the hyperfine couplings have opposite signs for the electrons in $d_{x^2-y^2}$ and in $d_{z^2}$, any admixture of these orbitals is expected to


dx.doi.org/10.1021/ic501869y | Inorg. Chem. 2014, 53, 12859−12869

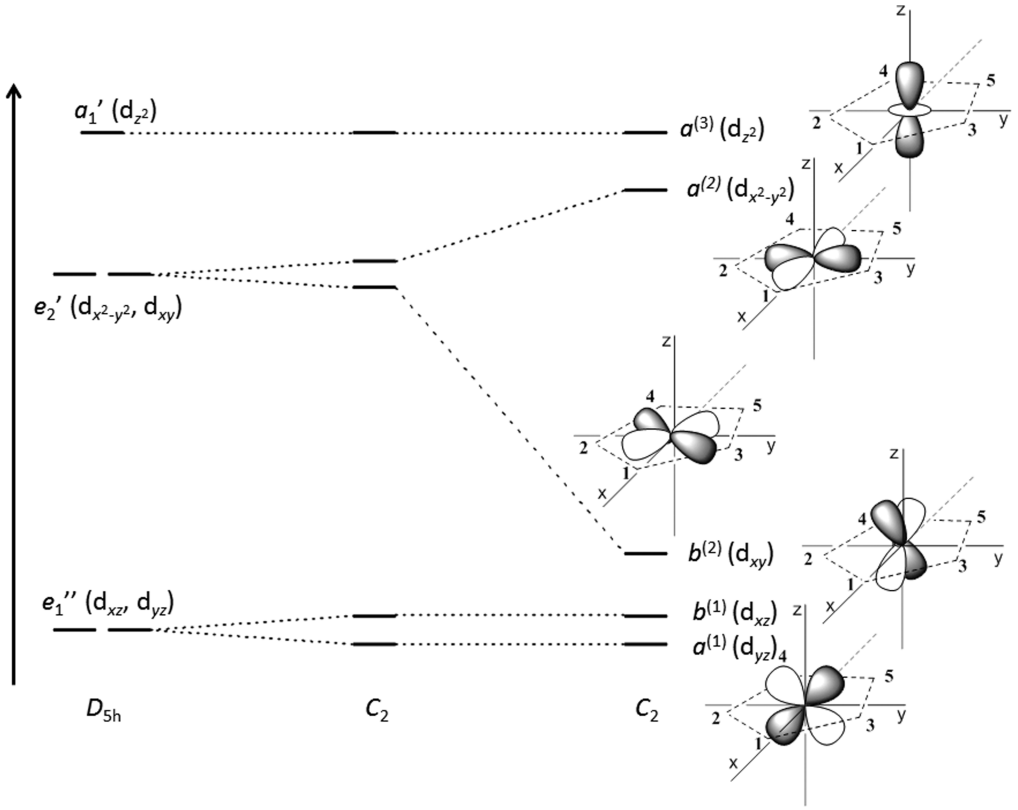


**Figure 6.** Qualitative diagram showing the splitting of the 3d orbitals of the metal ion in a pentagonal bipyramidal ligand field and the effect of lowering symmetry from $D_{5h}$ to $C_2$. The right-hand side of the diagram represents a $C_2$ symmetry such as that observed for [NiL$^1$], with two long M−donor distances (donor atoms in positions **4** and **5**) and a short M−donor distance (donor atom in position **1**).

**Table 3. $^1$H and $^{13}$C NMR Shifts (ppm with Respect to TMS) for [ZnL$^1$] at 298 K (pD ∼ 7.0) (see Chart 1 for Labeling)**

| $^1$H | | $^{13}$C | $\delta_i^{exp}$[a] | $\delta_i^{calcc}$ |
|---|---|---|---|---|
| H2ax | 3.10 | C1 | 180.6 | 179.4 |
| H2eq | 3.40 | C2 | 55.4 | 56.4 |
| H3ax | 3.08 | C3 | 59.3 | 62.0 |
| H3eq | 2.87 | C4 | 67.1 | 69.6 |
| H4ax | 3.41 | C5 | 69.9 | 71.9 |
| H4eq | 3.80 | C6 | 56.7 | 57.9 |
| H5ax | 3.59 | C7 | 65.1 | 66.8 |
| H5eq | 3.78 | | | |
| H6ax | 3.02 | | | |
| H6eq | 2.86 | | | |
| H7ax | 3.72 | | | |
| H7eq | 3.66 | | | |

[a]Assignment supported by 2D COSY, HSQC, and HMBC experiments at 298 K. [c]Calculated values obtained using the GIAO method.

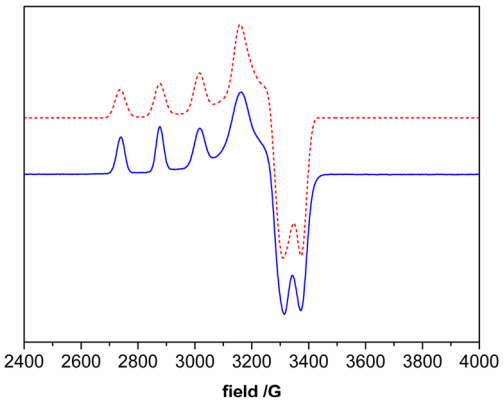


**Figure 7.** Experimental X-band EPR spectra (solid blue line) of the [CuL$^1$] complex in frozen water:DMSO (9:1 v/v) solution recorded at 90 K and the spectrum simulated (dashed red line) with the parameters given in Table 4. Experimental conditions: pH 7 and concentration *ca.* 1 mM. The microwave power was 2.0 mW, the modulation amplitude 1.0 mT, and the frequency ($\nu$) 9.51 GHz.

decrease the magnitude of $A_z$.[53] The analysis of the frontier $\beta$-MOs of the [CoL$^1$] and [CuL$^1$] complexes provides a plausible justification of observed EPR spectrum. The [CoL$^1$] complex shows an ordering of the $\beta$ frontier MOs that agrees with the qualitative predictions made on the basis of ligand-field theory.[54] The $\beta$ SOMOs with the highest energy are relatively close in energy (−5.62 and −5.32 eV) and contain important d metal contributions (83.9% and 73.4% according to Mulliken population analysis). These orbitals are correlated with the double-degenerate $e_1''$ orbitals in $D_{5h}$ symmetry, which correspond to the metal $d_{yz}$ and $d_{xz}$ orbitals (Figure 6). The $\beta$ LUMO and LUMO + 1 are also close in energy (−1.74 and −1.46 eV) and possess important 3d contribution (90.3% and 87.8%, respectively), dominated by the contribution of the metal $d_{xy}$ and $d_{x^2-y^2}$ orbitals (they correlate with the $e_2'$ orbitals in $D_{5h}$ symmetry). At higher energy is the $\beta$ LUMO + 2 (−0.06 eV) whose metal 3d contribution is dominated by the contribution of the $d_{z^2}$ orbital (Figure 8, see also Figure S10, Supporting Information). In the case of the [CuL$^1$] complex the $\beta$ LUMO is also dominated by the contribution of 3d orbitals (62.5%). Inspection of the $\beta$ HOMO + 2 of [CoL$^1$]


dx.doi.org/10.1021/ic501869y | *Inorg. Chem.* 2014, 53, 12859−12869

**Table 4. EPR Spectroscopic Parameters Obtained for [CuL$^1$] in Different Solvents**

| solvent | EPR params | | | | | |
|---|---|---|---|---|---|---|
| | $g_x$ | $g_y$ | $g_z$ | $A_x$[a] | $A_y$[a] | $A_z$[a] |
| Experimental | | | | | | |
| $H_2O$:DMSO;[b] pH = 7 | 2.043 | 2.106 | 2.307 | 26.6 | 26.8 | 149.8 |
| $H_2O$:glycerol;[b] pH = 7 | 2.041 | 2.112 | 2.308 | 26.3 | 30.4 | 149.2 |
| DMF | 2.035 | 2.107 | 2.294 | 20.8 | 28.3 | 151.7 |
| EtOH | 2.042 | 2.113 | 2.308 | 34.0 | 30.3 | 145.6 |
| Calculated[c] | | | | | | |
| $H_2O$, TPSSh | 2.031 | 2.070 | 2.144 | 1.5 | 55.9 | 156.9[d] |
| $H_2O$, BHLYP | 2.052 | 2.050 | 2.319 | 4.5 | 64.5 | 223.5[d] |

[a] $A_i \times 10^4$ (cm$^{-1}$). [b] 9:1 v/v. [c] Values obtained with DFT calculations (TPSSh or BHLYP functionals). [d] $A_z$ is calculated as a negative quantity.

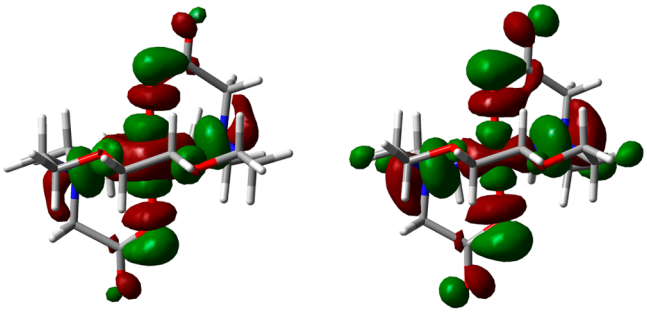


**Figure 8.** Surface plots of representative $\beta$ MOs obtained with DFT calculations for [CoL$^1$] (left) and [CuL$^1$] (right). Views are along the $C_2$ symmetry axes of the molecules. The different colors of the MOs indicate opposite signs of the wave function.

and the $\beta$ HOMO of [CuL$^1$], which are expected to be dominated by the contribution of the metal $d_{z^2}$ orbital, shows that they have similar shapes. However, it is also quite evident that for the [CuL$^1$] complex there is an important mixing of the $d_{x^2-y^2}$ and $d_{z^2}$ orbitals (Figure 8).

The EPR parameters of [CuL$^1$] were further investigated by calculating the *g*- and *A*-tensors using DFT computations (see Computational Methods section above for more information). These calculations used the geometry of the complex optimized at the TPSSh/TZVP level described above. Our calculations using the TPSSh functional provide a *g*-tensor with $g_z > g_y > g_x$ and $g_x = 2.03$, in agreement with the parameters obtained from the simulation of the experimental EPR spectrum. Thus, the calculated *g* values reproduce well the trend observed experimentally, although $g_y$ and particularly $g_z$ are underestimated by our DFT calculations. A similar methodology applied to tetragonal $Cu^{2+}$ complexes also showed underestimation of the calculated $g_z$ values, but reproduced correctly the observed experimental trends.[55] The calculated *A*-tensor gives an $A_z$ value in excellent agreement with the experiment ($157 \times 10^4$ cm$^{-1}$ vs $146-152 \times 10^4$ cm$^{-1}$ obtained experimentally), while the calculated $A_x$ and $A_y$ values also show reasonably good agreement with the experiment considering the difficulties associated with the accurate calculation of *A*-tensors. Recent benchmark studies have shown that the calculation of EPR parameters is very much dependent on the method employed, in particular on the functional used.[56] It has been shown that the accuracy of the calculated *g* values improves considerably upon increasing the amount of exact exchange. Calculations performed using the BHLYP functional (50% exact exchange) improve dramatically the agreement between the experimental and calculated $g_z$ values in comparison with the results obtained with the TPSSh functional (10% exchange). However, the BHLYP functional overestimates $A_z$ by a factor of 1.5 (Table 4), in line with previous results obtained with this functional.

Taken together, the reasonably good agreement obtained between the experimental and calculated EPR parameters confirms that the [CuL$^1$] complex presents a pentagonal bipyramidal coordination in solution similar to that found in the X-ray structure. The presence of three long Cu−O bond lengths in the equatorial plane of the pentagonal bipyramid approaches the metal coordination environment to a square planar coordination, for which a $g_z > g_y > g_x$ trend is expected.

**Stability Trends across the First-Row Transition Series.** The evolution of the stability of [ML$^1$] complexes (M = Co, Ni, Cu, or Zn) was analyzed by calculating the free energy ($\Delta G_g$) for the following reaction:

$$[CoL^1](g) + [M(H_2O)_6]^{2+}(g) \rightarrow [ML^1](g) + [Co(H_2O)_6]^{2+}(g) \quad \text{with M = Ni, Cu, or Zn} \qquad (1)$$

In these calculations we used the geometries of the complexes optimized at the TPSSh/TZVP level in the gas phase, which present bond distances of the metal coordination environments very similar to those obtained in aqueous solution (Table S1, Supporting Information). A similar methodology has been recently proposed to analyze stability trends of lanthanide complexes across the 4f period.[57] In the latter case, the naked $Ln^{3+}$ ions were used for the energy analysis due to the core nature of the 4f electrons and the electrostatic character of the metal−ligand(s) bonds. For transition metal complexes the 3d orbitals are involved in covalent chemical bonding, and therefore it is more adequate to include an explicit first coordination shell. This analysis allows the evaluation of stability trends for closely related complexes, instead of the energy changes for the complexation process of the individual [ML$^1$] complexes. Such analysis has been undertaken for $[M(edta)]^{2-}$ complexes by Ma et al.,[58] but the quantitative agreement of the experimental and calculated complexation free energies was found to be rather poor, with deviations of up to 18 kcal mol$^{-1}$. We believe that this disagreement is mainly caused by the inaccurate hydration free energies of the $edta^{4-}$ ligand obtained with the PCM model, which is known to have serious limitations to predict the hydration energies of solutes with concentrated charge densities.[59]

The geometries of the $[M(H_2O)_6]^{2+}$ (M = Co, Ni, or Zn) complexes optimized in the gas phase at the TPSSh/TZVP level present nearly undistorted octahedral coordination environments with the following bond distances: Co−O = 2.112(1) Å, Ni−O = 2.070(1) Å, and Zn−O = 2.112(1) Å. These values are close to those obtained both experimentally and in previous computational studies.[60] As expected, for the $[Cu(H_2O)_6]^{2+}$ complex the optimized geometry shows a Jahn−Teller distorted octahedral coordination with equatorial bond lengths of 2.017(5) Å and two elongated axial Cu−O bonds of 2.276 Å. These distances are also in good agreement with typical experimental and theoretical values.[61]


dx.doi.org/10.1021/ic501869y | Inorg. Chem. 2014, 53, 12859−12869

The calculated $\Delta G_g$ values, which are provided in Table 5 and Figure 9, include BSSE corrections that arise from the

**Table 5. Calculated Gibbs Free Energies for Reactions 1 and 2[a]**

| $M^{2+}$ | $\Delta G_g$ | $\Delta G_{aq}^{calcd}$ | $\Delta G_{aq}^{exptl}$ |
|---|---|---|---|
| Co | 0.00 | 0.00 | 0.00 |
| Ni | 4.33 | 1.74 | 1.84 |
| Cu | −16.68 | −10.73 | −5.56 |
| Zn | −0.60 | 0.05 | −0.98 |

[a]Values are in kcal $mol^{-1}$.

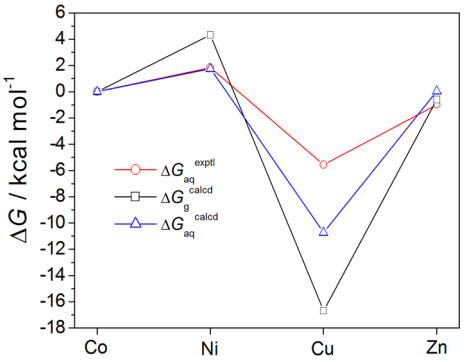


**Figure 9.** Comparison of the $\Delta G_g$ and $\Delta G_{aq}^{calcd}$ values obtained with DFT calculations and the experimental values ($\Delta G_{aq}^{exptl}$) obtained from the corresponding stability constants.

formation of the M−$L^1$ and Co−$OH_2$ bonds and the breaking of the Co−$L^1$ and M−$OH_2$ bonds. BSSEs for the $[M(H_2O)_6]^{2+}$ complexes were found to vary in the order $Co^{2+} < Ni^{2+} < Cu^{2+} \gg Zn^{2+}$. However, in the case of the $[ML^1]$ complexes this trend is different, as the BSSE calculated for the complex of $Ni^{2+}$ is slightly lower than that of the $Co^{2+}$ analogue (Table S2, Supporting Information).

The $\Delta G_g$ values present a quite good agreement with the experimental $\Delta G_{aq}$ obtained from the stability constants determined potentiometrically (Figure 9 and Table 5). The experimental trend is very well-reproduced, although the absolute deviations between experimental and calculated values obtained for the complexes of $Ni^{2+}$ and $Cu^{2+}$ are relatively large (2.5 and 11.1 kcal $mol^{-1}$, respectively).

The evolution of the stability of $[ML^1]$ complexes was also evaluated in aqueous solution by calculating the Gibbs energy ($\Delta G_{aq}$) for reaction 2:

$$[CoL^1](sol) + [M(H_2O)_6]^{2+}(sol) \rightarrow [ML^1](sol) + [Co(H_2O)_6]^{2+}(sol) \quad \text{with M = Ni, Cu, or Zn} \tag{2}$$

In these calculations the geometries of $[ML^1]$ and $[M(H_2O)_6]^{2+}$ complexes optimized in aqueous solution were used. The inclusion of solvent effects has a minor impact in the bond distances of the $[M(H_2O)_6]^{2+}$ complexes, which take the following values in aqueous solution: Co−O = 2.095(1) Å, Ni−O = 2.063(1) Å, Cu−O = 2.274(1) Å (axial) and 2.012(1) Å (equatorial), Zn−O = 2.103(1) Å. The inclusion of solvent effects causes a significant improvement of the agreement between the experimental and calculated free energy values (Figure 9). The $\Delta G_{aq}^{calcd}$ values calculated for $[NiL^1]$ and $[ZnL^1]$ show an excellent quantitative agreement with the experiment (within ca. 1 kcal $mol^{-1}$). For the $Cu^{2+}$ complex the deviation is somewhat larger (~5.2 kcal $mol^{-1}$). This larger deviation could arise from different sources, such as the experimental errors in stability constant determination, the effect of the electrolyte used to keep constant the ionic strength in potentiometric measurements, or intrinsic errors of the computational methodology used (density functional, basis sets, and solvation model). However, an inadequate description of $Cu^{2+}$ solvation might be also behind the poorer agreement obtained for this ion. Indeed, the coordination geometry of $Cu^{2+}$ ions in aqueous solution is still a matter of debate, with different authors proposing solution structures with a Jahn−Teller distorted $[Cu(H_2O)_6]^{2+}$ coordination,[62] a 5-fold coordination,[63] or even a tetrahedral coordination.[64]

The similar stability trends predicted in the gas phase and in solution indicate that solvent effects play a minor role in the relative stability of this family of complexes. The reversed stability of the $Co^{2+}$ and $Ni^{2+}$ complexes is clearly related to an unfavorable distribution of the metal 3d electrons of $Ni^{2+}$ in a pentagonal bipyramidal coordination, which gives an ordering of the metal 3d orbitals such that $d_{z^2} > d_{x^2-y^2}$, $d_{xy} > d_{xz}, d_{yz}$. A $d^8$ configuration results in an unequal occupation of the $d_{x^2-y^2}$ and $d_{xy}$ orbitals, which are strictly degenerate in $D_{5h}$ symmetry (Figure 6). Since the abundance of seven coordination for $Co^{2+}$, $Ni^{2+}$, $Co^{2+}$, and $Zn^{2+}$ is low, it is clear that pentagonal bipyramidal complexes can only be formed with preorganized ligands that favor this geometry. The analysis of the potential energy surface of $[NiL^1]$ (Figures 4 and 5) indicates that the distortion associated with the Jahn−Teller effect involves changes of the Ni−O distances to donor atoms of the equatorial plane. However, such nuclear displacements might be constrained by the macrocyclic structure of the ligand, which holds together the five donor atoms of the equatorial plane. If so, the distortion of the metal coordination environment imposed by the Jahn−Teller effect in the corresponding complexes of $Ni^{2+}$ would have an important impact in the stability of the complex, which should decrease significantly.

## CONCLUSIONS

In this work we have shown that the $[ML^1]$ complexes (M = Co, Ni, Cu, or Zn) adopt seven-coordinate structures both in the solid state and in solution, with the structure of the $[NiL^1]$ complex suffering a significant distortion associated with a pseudodegenerate electronic ground state. Distorted seven-coordinate or six-coordinate geometries were previously observed for $Ni^{2+}$ complexes with related ligands.[12−17] An unfavorable distribution of the metal 3d electrons of $Ni^{2+}$ in pentagonal bipyramidal coordination is responsible for the low abundance of seven-coordinate complexes of this metal ion, when compared with other first-row transition metal ions. In this Article, we have shown that this unfavorable electron distribution has an important impact on the stability trend observed for $[ML^1]$ complexes, as the complex of $Ni^{2+}$ is less stable than those of $Co^{2+}$, $Cu^{2+}$, and $Zn^{2+}$. Furthermore, DFT calculations have been shown to reproduce fairly well the experimental stability trend. This paves the way for the accurate prediction of complex stabilities, which might be very helpful to aid ligand design. The results reported here show that ligands preorganized to give pentagonal bipyramidal coordination can be used for the selective complexation of $Co^{2+}$ and $Zn^{2+}$ over $Ni^{2+}$, an issue of great importance in hydrometallurgy.


dx.doi.org/10.1021/ic501869y | Inorg. Chem. 2014, 53, 12859−12869

## ■ ASSOCIATED CONTENT

### Supporting Information

X-ray crystallographic data in CIF format, HR-MS, electronic absorption spectra, NMR spectra, BSSEs, calculated bond distances, and optimized Cartesian coordinates (Å) of the complexes obtained with DFT calculations. This material is available free of charge via the Internet at http://pubs.acs.org.

## ■ AUTHOR INFORMATION


### Corresponding Author

*E-mail: carlos.platas.iglesias@udc.es.


### Notes

The authors declare no competing financial interest.

## ■ ACKNOWLEDGMENTS

The authors thank Xunta de Galicia (CN2012/011) and Universidade da Coruña for financial support. The authors are indebted to Centro de Supercomputación de Galicia (CESGA) and Centro de Servicios de Informatica y Redes de Comunicaciones (CSIRC), Universidad de Granada, for providing the computer facilities. V. B. thanks Ministerio de Economía y Competitividad (Spain) for a "Juan de la Cierva" postdoctoral contract. The authors also acknowledge Fundação para a Ciência e a Tecnologia (FCT) for the financial support under Project PTDC/QEQ-SUP/2718/2012 and for the postdoctoral fellowship of L.M.P.L. (SFRH/BPD/73361/2010).

## ■ REFERENCES


(1) Casanova, D.; Alemany, P.; Bofill, J. M.; Alvarez, S. *Chem.—Eur. J.* **2003**, *9*, 1281−1295.

(2) The Cambridge Structural Database (version 5.35): Allen, F. H. *Acta Crystallogr.* **2002**, *B58*, 380−388.

(3) ConQuest (version 1.16): Bruno, I. J.; Cole, J. C.; Edgington, P. R.; Kessler, M.; Macrae, C. F.; McCabe, P.; Pearson, J.; Taylor, R. *Acta Crystallogr.* **2002**, *B58*, 389−397.

(4) CSD searches were performed with the following restrictions: As donor atoms we considered N, P, O, S, and any element of group 17. Structures with agreement factors $R > 0.075$, polynuclear structures, and disordered structures were disregarded. Metal−donor distances < 2.5 Å have been considered. Using thresholds of 2.4 or 2.7 Å does not alter the overall trend (see Supporting Information).

(5) (a) Maigut, J.; Meier, R.; Zahl, A.; van Eldik, R. *J. Am. Chem. Soc.* **2008**, *130*, 14556−14569. (b) Maigut, J.; Meier, R.; Zahl, A.; van Eldik, R. *Inorg. Chem.* **2007**, *46*, 5361−5371. (c) Rolla, G. A.; Platas-Iglesias, C.; Botta, M.; Tei, L.; Helm, L. *Inorg. Chem.* **2013**, *52*, 3268−3279. (d) Meier, R.; Platas-Iglesias, C.; Heinemann, F. W.; Linti, G.; Schulte, J.; Srivastava, S. K. *Inorg. Chem.* **2014**, *53*, 6684−6697.

(6) Delgado, R.; Fraústo da Silva, J. J. R.; Vaz, M. C. T. A. *Polyhedron* **1987**, *6*, 29−38.

(7) Chang, C. A.; Ochaya, V. O. *Inorg. Chem.* **1986**, *25*, 355−358.

(8) Delgado, R.; Fraústo da Silva, J. J. R.; Vaz, M. C. T. A.; Paoletti, P.; Micheloni, M. *J. Chem. Soc., Dalton Trans.* **1989**, 133−137.

(9) (a) Lacoste, R. G.; Christoffers, G. V.; Martell, A. E. *J. Am. Chem. Soc.* **1965**, *87*, 2385−2388. (b) Martell, A. E.; Motekaitis, R. J.; Smith, R. M. *NIST Critically Selected Stability Constants of Metal Complexes Database, Version 8.0 for Windows*; National Institute of Standards and Technology, Standard Reference Data Program: Gaithersburg, MD, 2004.

(10) Urbanczyk-Lipkowska, Z.; Gluzinski, P.; Krajewski, J. W.; Kolinski, R. A. *J. Cryst. Spectrosc.* **1989**, *19*, 387−397.

(11) Mateus, P.; Li, F.; Esteves, C. V.; Delgado, R.; Brandão, P.; Felix, V. *Eur. J. Inorg. Chem.* **2011**, 4700−4708.

(12) Platas-Iglesias, C.; Vaiana, L.; Esteban-Gomez, D.; Avecilla, F.; Real, J. A.; de Blas, A.; Rodriguez-Blas, T. *Inorg. Chem.* **2005**, *44*, 9704−9713.

(13) Vaiana, L.; Regueiro-Figueroa, M.; Mato-Iglesias, M.; Platas-Iglesias, C.; Esteban-Gomez, D.; de Blas, A.; Rodriguez-Blas, T. *Inorg. Chem.* **2007**, *46*, 8271−8282.

(14) Vaiana, L.; Platas-Iglesias, C.; Esteban-Gomez, D.; Avecilla, F.; de Blas, A.; Rodriguez-Blas, T. *Eur. J. Inorg. Chem.* **2007**, 1874−1883.

(15) Rodriguez-Infante, C.; Esteban, D.; Avecilla, F.; de Blas, A.; Rodríguez-Blas, T.; Mahia, J.; Macedo, A. L.; Geraldes, C. F. G. C. *Inorg. Chim. Acta* **2001**, *317*, 190−198.

(16) Vaiana, L.; Esteban-Gomez, D.; Platas-Iglesias, C.; Mato-Iglesias, M.; Avecilla, F.; de Blas, A.; Rodriguez-Blas, T. *Polyhedron* **2007**, *26*, 4141−4146.

(17) (a) Olatunde, A. O.; Dorazio, S. J.; Spernyak, J. A.; Morrow, J. R. *J. Am. Chem. Soc.* **2012**, *134*, 18503−18505. (b) Olatunde, A. O.; Cox, J. M.; Daddario, M. D.; Spernyak, J. A.; Benedict, J. B.; Morrow, J. R. *Inorg. Chem.* **2014**, *53*, 8311−8321.

(18) Selmeczi, K.; Joly, J.-P.; Allali, M.; Yeguas, V.; Henry, B.; Ruiz-Lopez, M. *Eur. J. Inorg. Chem.* **2014**, 4934−4945.

(19) Hendrich, M. P. *SpinCount Software*; Carnegie Mellon University: Pittsburgh, PA; available at http://www.chem.cmu.edu/groups/hendrich/.

(20) Sheldrick, G. M. *SADABS Version 2.10*; University of Göttingen: Göttingen, Germany, 2004.

(21) SHELX Sheldrick, G. M. *Acta Crystallogr.* **2008**, *A64*, 112−122.

(22) Farrugia, L. J. *J. Appl. Crystallogr.* **1999**, *32*, 837−838.

(23) Beurskens, P. T.; Beurskens, G.; Gelder, R.; Smits, J. M. M.; Garcia-Granda, S.; Gould, R. O. *DIRDIF-2008—A Computer Program for Crystal Structure Determination by Patterson Methods and Direct Methods Applied to Difference Structure Factors*; Crystallography Laboratory, Radbound University Nijmegen: Nijmegen, The Netherlands, 2008.

(24) Flack, H. D. *Acta Crystallogr.* **1983**, *A39*, 876−881.

(25) (a) Le Page, Y. *J. Appl. Crystallogr.* **1987**, *20*, 264−269. (b) Le Page, Y. *J. Appl. Crystallogr.* **1988**, *21*, 983−984.

(26) Tao, J. M.; Perdew, J. P.; Staroverov, V. N.; Scuseria, G. E. *Phys. Rev. Lett.* **2003**, *91*, 146401.

(27) Frisch, M. J.; Trucks, G. W.; Schlegel, H. B.; Scuseria, G. E.; Robb, M. A.; Cheeseman, J. R.; Scalmani, G.; Barone, V.; Mennucci, B.; Petersson, G. A.; Nakatsuji, H.; Caricato, M.; Li, X.; Hratchian, H. P.; Izmaylov, A. F.; Bloino, J.; Zheng, G.; Sonnenberg, J. L.; Hada, M.; Ehara, M.; Toyota, K.; Fukuda, R.; Hasegawa, J.; Ishida, M.; Nakajima, T.; Honda, Y.; Kitao, O.; Nakai, H.; Vreven, T.; Montgomery, J. A., Jr.; Peralta, J. E.; Ogliaro, F.; Bearpark, M.; Heyd, J. J.; Brothers, E.; Kudin, K. N.; Staroverov, V. N.; Kobayashi, R.; Normand, J.; Raghavachari, K.; Rendell, A.; Burant, J. C.; Iyengar, S. S.; Tomasi, J.; Cossi, M.; Rega, N.; Millam, N. J.; Klene, M.; Knox, J. E.; Cross, J. B.; Bakken, V.; Adamo, C.; Jaramillo, J.; Gomperts, R.; Stratmann, R. E.; Yazyev, O.; Austin, A. J.; Cammi, R.; Pomelli, C.; Ochterski, J. W.; Martin, R. L.; Morokuma, K.; Zakrzewski, V. G.; Voth, G. A.; Salvador, P.; Dannenberg, J. J.; Dapprich, S.; Daniels, A. D.; Farkas, Ö.; Foresman, J. B.; Ortiz, J. V.; Cioslowski, J.; Fox, D. J. *Gaussian 09, Revision A.01*; Gaussian, Inc.: Wallingford, CT, 2009.

(28) Schaefer, A.; Huber, C.; Ahlrichs, R. *J. Chem. Phys.* **1994**, *100*, 5829−5835.

(29) Stanton, J. F.; Gauss, J. *Adv. Chem. Phys.* **2003**, *125*, 101−146.

(30) Montoya, A.; Truong, T. N.; Sarofim, A. F. *J. Phys. Chem. A* **2000**, *104*, 6108−6110.

(31) Tomasi, J.; Mennucci, B.; Cammi, R. *Chem. Rev.* **2005**, *105*, 2999−3093.

(32) Bernardi, F.; Boys, S. F. *Mol. Phys.* **1970**, *19*, 553−566.

(33) Zawada, A.; Gora, R. W.; Mikolajczyk, M. M.; Bartkowiak, W. *J. Phys. Chem. A* **2012**, *116*, 4409−4416.

(34) Wolinski, K.; Hilton, J. F.; Pulay, P. *J. Am. Chem. Soc.* **1990**, *112*, 8251−8260.

(35) Neese, F. *Wiley Interdiscip. Rev.: Comput. Mol. Sci.* **2012**, *2*, 73−78.

(36) (a) Neese, F. *J. Chem. Phys.* **2003**, *117*, 3939−3948. (b) Neese, F. *J. Chem. Phys.* **2001**, *115*, 11080−11096. (c) Neese, F. *J. Phys. Chem. A* **2001**, *105*, 4290−4299.
(37) Kossmann, S.; Kirchner, B.; Neese, F. *Mol. Phys.* **2007**, *105*, 2049−2070.
(38) (a) Lee, C.; Yang, W.; Parr, R. G. *Phys. Rev. B* **1988**, *37*, 785−789. (b) Becke, A. D. *J. Chem. Phys.* **1993**, *98*, 1372−1377.
(39) Neese, F. *J. Chem. Phys.* **2005**, *122*, 034107.
(40) The CP basis is based on the TurboMole DZ basis developed by Ahlrichs and co-workers and obtained from the basis set library under ftp.chemie.unikarlsruhe.de/pub/basen.
(41) Schaefer, A.; Horn, H.; Ahlrichs. *J. Chem. Phys.* **1992**, *97*, 2571−2577.
(42) Krishnan, R.; Binkley, J. S.; Seeger, R.; Pople, J. A. *J. Chem. Phys.* **1980**, *72*, 650−654.
(43) Kossmann, S.; Neese, F. *Chem. Phys. Lett.* **2009**, *481*, 240−243.
(44) Weigend, F.; Ahlrichs, R. *Phys. Chem. Chem. Phys.* **2005**, *7*, 3297−3305.
(45) Sinnecker, S.; Rajendran, A.; Klamt, A.; Diedenhofen, M.; Neese, F. *J. Phys. Chem. A* **2006**, *110*, 2235−2245.
(46) (a) Achilefu, S.; Wilhelm, R. R.; Jimenez, H. N.; Schmidt, M. A.; Srinivasan, A. *J. Org. Chem.* **2000**, *65*, 1562−1565. (b) Platas-Iglesias, C.; Mato-Iglesias, M.; Djanashvili, K.; Muller, R. N.; Vander Elst, L.; Peters, J. A.; de Blas, A.; Rodríguez-Blas, T. *Chem.—Eur. J.* **2004**, *10*, 3579−3590.
(47) Llunell, M.; Casanova, D.; Cirera, J.; Alemany, P.; Alvarez, S. *SHAPE. Program for the Stereochemical Analysis of Molecular Fragments by Means of Continuous Shape Measures and Associated Tools, Version 2.1*.
(48) (a) Pinsky, M.; Avnir, D. *Inorg. Chem.* **1998**, *37*, 5575−5582. (b) Casanova, D.; Cirera, J.; Llunell, M.; Alemany, P.; Avnir, D.; Alvarez, S. *J. Am. Chem. Soc.* **2004**, *126*, 1755−1763. (c) Cirera, J.; Ruiz, E.; Alvarez, S. *Chem.—Eur. J.* **2006**, *12*, 3162−3167.
(49) Bersuker, I. B. *Chem. Rev.* **2001**, *101*, 1067−1114.
(50) Panda, M.; Phuan, P.-W.; Kozlowski, M. C. *Chem. Commun.* **2002**, 1552−1553.
(51) (a) Hathaway, B. J.; Tomlinson, A. A. G. *Coord. Chem. Rev.* **1970**, *5*, 1−43. (b) Hathaway, B. J.; Billing, D. E. *Coord. Chem. Rev.* **1970**, *5*, 143−207. (c) Lever, A. B. P. *Inorganic Electronic Spectroscopy*, 2nd ed.; Elsevier: Amsterdam, 1984; pp 554−572.
(52) Hathaway, B. J. *Coord. Chem. Rev.* **1983**, *52*, 87−169.
(53) (a) Attanasio, D. *J. Magn. Reson.* **1977**, *26*, 81−91. (b) Srinivas, D.; Swamy, M. V. B. L.; Subramanian, S. *Mol. Phys.* **1986**, *57*, 55−63. (c) Benial, A. M. F.; Ramakrishnan, V.; Murugesan, R. *Spectrochim. Acta* **2000**, *A56*, 2775−2781. (d) Karunakaran, C.; Justin Thomas, K. R.; Shunmugasundaram, A.; Murugesan, R. *Spectrochim. Acta* **2001**, *A57*, 441−449. (e) Valach, F.; Grobelny, R.; Glowiak, T.; Mrozinski, J.; Lukeš, V.; Blahova, Z. *J. Coord. Chem.* **2010**, *63*, 1645−1651.
(54) Hoffmann, R.; Beier, B. F.; Muetterties, E. L.; Rossi, A. R. *Inorg. Chem.* **1977**, *16*, 511−522.
(55) Ames, W. M.; Larsen, S. C. *J. Phys. Chem. A* **2009**, *113*, 4305−4312.
(56) de Visser, S. P.; Quesne, M. G.; Martin, B.; Comba, P.; Ryde, U. *Chem. Commun.* **2014**, *50*, 262−282.
(57) Regueiro-Figueroa, M.; Esteban-Gómez, D.; de Blas, A.; Rodríguez-Blas, T.; Platas-Iglesias, C. *Chem.—Eur. J.* **2014**, *20*, 3974−3981.
(58) Chen, L.; Liu, T.; Ma, C. *J. Phys. Chem. A* **2010**, *114*, 443−454.
(59) (a) Bryantsev, V. S.; Diallo, M. S.; Goddard, W. A., III. *J. Phys. Chem. A* **2009**, *113*, 9559−9567. (b) Gutowski, K. E.; Dixon, D. A. *J. Phys. Chem. A* **2006**, *110*, 8840−8856.
(60) Akesson, R.; Pettersson, L. G. M.; Sandstrom, M.; Wahlgren, U. *J. Am. Chem. Soc.* **1994**, *116*, 8691−8704.
(61) (a) de Almeida, K. J.; Rinkevicius, Z.; Hugosson, H. W.; Ferreira, A. C.; Agren, H. *Chem. Phys.* **2007**, *332*, 176−187. (b) Ohtaki, H.; Radnai, T. *Chem. Rev.* **1993**, *93*, 1157−1204.
(62) Gómez-Salces, S.; Aguado, F.; Valiente, R.; Rodríguez, F. *Angew. Chem., Int. Ed.* **2012**, *51*, 9335−9338.
(63) Pasquarello, A.; Petri, I.; Salmon, P. S.; Parisel, O.; Car, R.; Tóth, É.; Powell, D. H.; Fishcher, H. E.; Helm, L.; Merbach, A. E. *Science* **2001**, *291*, 856−859.
(64) Bowron, D. T.; Amboage, M.; Boada, R.; Freeman, A.; Hayama, S.; Díaz-Moreno, S. *RSC Adv.* **2013**, *3*, 17803−17812.